

Time-dependent approach to many-particle tunneling in one dimensionTakahito Maruyama,^{1,*} Tomohiro Oishi,¹ Kouichi Hagino,¹ and Hiroyuki Sagawa^{2,3}¹*Department of Physics, Tohoku University, Sendai 980-8578, Japan*²*Center for Mathematics and Physics, University of Aizu, Aizu-Wakamatsu, Fukushima 965-8560, Japan*³*RIKEN Nishina Center, Wako 351-0198, Japan*

(Received 6 July 2012; published 1 October 2012)

By employing the time-dependent approach, we investigate a quantum tunneling decay of many-particle systems. We apply it to a schematic one-dimensional three-body model with a heavy-core nucleus and two valence protons. We calculate the decay width for two-proton emission from the survival probability, which well obeys the exponential decay law after a sufficient time. The effect of the correlation between the two emitted protons is also studied by observing the time evolution of the two-particle density distribution. It is shown that the pairing correlation significantly enhances the probability for the simultaneous diproton decay.

DOI: [10.1103/PhysRevC.86.044301](https://doi.org/10.1103/PhysRevC.86.044301)

PACS number(s): 23.50.+z, 23.60.+e, 21.45.-v, 03.65.Xp

I. INTRODUCTION

The quantum tunneling of a system with intrinsic degrees of freedom or of many particles is an important subject of modern physics [1–6]. In nuclear physics, typical examples include heavy-ion fusion reactions at sub-barrier energies [7,8], spontaneous fission [9], α and heavy-cluster decays [10], and stellar nucleosynthesis [11,12]. In heavy-ion fusion reactions, for instance, it has been well recognized that the couplings of the relative motion between the colliding nuclei to several collective motions enhance the tunneling probability of the Coulomb barrier, thus, increasing the fusion cross sections by several orders of magnitude as compared to the prediction of a simple potential model [7,8]. Nevertheless, it has still been a challenging problem to understand the many-particle tunneling from a fully microscopic view. For instance, even though there have been several attempts [10,13–15], α decays have not fully been understood microscopically with sufficient accuracy.

Recently, two-proton ($2p$) radioactivities have been experimentally observed for a few proton-rich nuclei outside the proton drip line, such as ^{45}Fe [16–18] and ^6Be [19–21], and have attracted much attention [22–25] in connection with, e.g., the dinucleon correlations [26–29]. This is a phenomenon of spontaneous emission of two valence protons from the parent proton-rich nuclei in which the emission of one proton is energetically forbidden. Notice that an analogous process of the two-proton radioactivity, that is, a two-neutron decay has also been observed recently for ^{16}Be [30]. These two-nucleon emission decays may provide a useful testing ground for many-particle tunneling theories.

The primary task for a many-particle tunneling decay is to investigate the effect of interaction or correlation among emitted particles on decay properties, such as the decay width and the survival probability. In the case of $2p$ decay, this corresponds to the pairing correlation between the valence

protons. Because of the strong pairing correlation in proton-rich nuclei, $2p$ emitters are expected to have an even number of protons outside the proton drip line. Incidentally, it has been well known that the pairing correlation plays an important role in two-neutron transfer reactions [31–33].

The quantum tunneling decay phenomena can be studied either with the time-independent approach [10,24,25] or with the time-dependent approach [34–40]. In the time-independent approach, one seeks, e.g., a Gamow state, which is a purely outgoing wave outside the barrier. The imaginary part of the energy of the Gamow state is related to the decay width, whereas, the real part corresponds to the resonance energy. On the other hand, in the time-dependent approach, one first modifies the potential barrier so that the initial state can be prepared as a bound state of a confining potential. The confining potential is then suddenly changed to the original barrier, and the initial state evolves in time. The decay width can be obtained from the survival probability of the initial state. An advantage of the time-independent approach is that the decay width can be calculated with high accuracy even when the decay width is extremely small [41]. An advantage of the time-dependent approach, on the other hand, is that it provides an intuitive way to understand the tunneling decay, even though it may be difficult to apply it to a situation with an extremely small decay width. This approach may provide a useful means to explore the mechanism of many-particle tunneling decay, although it has, so far, been applied only to two-body decay phenomena, such as α decays and one-proton decays [34–38].

In this paper, we extend the time-dependent approach to two-proton emissions and discuss the dynamics of a two-particle tunneling decay. To this end, we employ the schematic one-dimensional three-body model [42], which consists of a heavy-core nucleus and two valence protons. We solve the time-dependent Schrödinger equation by expanding the wave function on a basis with time-dependent expansion coefficients. The decay width is then defined from the survival probability. We will study the time evolution of the survival probability as well as the density distribution. We will also discuss the role of the pairing correlation in the two-proton decay.

*Present address: Fusion Research and Development Directorate, Japan Atomic Energy Agency (JAEA), Naka, Ibaraki 311-0193, Japan.

The paper is organized as follows. In Sec. II, we detail our formalism for the time-dependent approach to the two-proton decays. We show the results of the calculations in Sec. III. It will be shown that the decay width will converge to a constant value after a sufficient time evolution, which will indicate that the decay rate will follow the exponential law. With this method, the time evolution of a quasistationary $2p$ state, namely, the density and the flux distributions, can be visualized. By using them, we will discuss an important role of the pairing interaction between the two protons in the decay process. Finally, we summarize the paper in Sec. IV.

II. FORMALISM

A. One-dimensional three-body model

We consider a one-dimensional three-body system with two valence protons and the core nucleus whose atomic and mass numbers are Z_c and A_c , respectively. By neglecting the recoil kinetic energy of the core nucleus, the three-body Hamiltonian reads [42]

$$H = h(x_1) + h(x_2) + v_{pp}(x_1, x_2), \quad (1)$$

$$h(x) = -\frac{\hbar^2}{2m} \frac{d^2}{dx^2} + V(x), \quad (2)$$

where m is the nucleon mass and x_1 and x_2 are the coordinates of the valence protons with respect to the core nucleus. $V(x)$ is the potential between a valence proton and the core, whereas, $v_{pp}(x_1, x_2)$ is the interaction between the two valence protons. The core-proton potential,

$$V(x) = V_{\text{nuc}}(x) + V_{\text{coul}}(x) \quad (3)$$

consists of the nuclear part V_{nuc} and the Coulomb part V_{coul} . For the nuclear part, we take a Woods-Saxon form,

$$V_{\text{nuc}}(x) = -\frac{V_0}{1 + e^{(|x|-R)/a}}. \quad (4)$$

For the Coulomb part, we employ a soft-core Coulomb potential [43–45], that is,

$$V_{\text{coul}}(x) = \frac{Z_c e^2}{\sqrt{b^2 + x^2}}. \quad (5)$$

In this paper, we take $V_0 = 46.5$ MeV. The radius R and the surface diffuseness parameter a in the Woods-Saxon potential, Eq. (4), are taken to be $R = 1.27 A_c^{1/3}$ and $a = 0.67$ fm, respectively. We arbitrarily take $A_c = 60$ and $Z_c = 30$ for the mass and atomic numbers of the core nucleus, whereas, we use $b = 2.0$ fm in the Coulomb interaction.

The interaction $v_{pp}(x_1, x_2)$ induces the pairing correlation between the two valence protons. In this paper, we adopt a density-dependent contact interaction of the surface type [42], that is,

$$v_{pp}(x_1, x_2) = -g \left(1 - \frac{1}{1 + e^{(|\bar{x}|-R)/a}} \right) \delta(x_1 - x_2), \quad (6)$$

where g is the strength of the interaction and $\bar{x} = (x_1 + x_2)/2$. The density dependence is introduced with the Woods-Saxon form [R and a are the same as those in Eq. (4)]. Notice

that, in the limit of $|\bar{x}| \rightarrow \infty$, this interaction becomes a pure contact interaction, $-g\delta(x_1 - x_2)$. For simplicity, we neglect the Coulomb interaction between the two protons. We have confirmed that, as long as the one-dimensional three-body system is concerned, its effect on the decay properties can be well taken into account by somewhat reducing the strength g (see also Refs. [29,46,47]).

It is important to notice that a one-dimensional δ function potential $v(x) = -g\delta(x)$ always holds a bound state at $E_{pp} = -mg^2/4\hbar^2$ for a two-proton system even with an infinitesimally small attraction g [48]. This is in contrast to a three-dimensional system in which a bound state exists only with a strong strength g of an attractive contact interaction.

B. Time-dependent method

To describe the $2p$ tunneling, we employ the time-dependent method. The first step is to prepare the initial $2p$ state, which is confined inside the potential barrier as in the two-potential method developed by Gurvitz and Kalbermann [49], Gurvitz [50], and Gurvitz *et al.* [51]. To this end, we modify the core-proton potential $V(x)$ to a confining potential $V_{\text{mod}}(x)$ defined as

$$\begin{aligned} V_{\text{mod}}(x) &= V(x), & |x| \leq |x_c| \\ &= V(x_c), & |x| > |x_c|. \end{aligned} \quad (7)$$

In Fig. 1, we show the confining potential V_{mod} and the original potential V together with the wave function for the bound state of V_{mod} . The position x_c can be chosen arbitrarily as long as $V(x_c)$ is larger than the resonance energy, although the accuracy is improved if x_c is chosen so that $V(x_c)$ is as close as possible to the resonance energy [51]. When this condition is satisfied, the modified potential V_{mod} holds a bound state, which resembles the resonance state of the original potential. In this paper, we choose $x_c = 10$ fm, which yields the bound state at $\epsilon = 2.71$ MeV for the modified

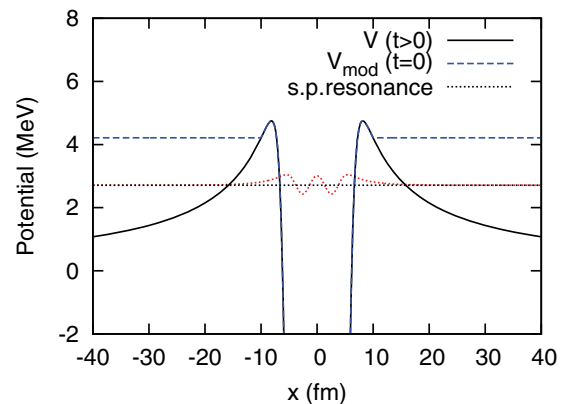


FIG. 1. (Color online) The core-proton potential used in our calculations. The initial state at $t = 0$ is constructed with a modified potential $V_{\text{mod}}(x)$ given by Eq. (7), which is shown by the dashed line. For $t > 0$, the potential is changed to the original potential $V(x)$, given by Eq. (3) as shown by the solid line. We also show the wave function for the bound single particle (s.p.) state of the modified potential at $\epsilon = 2.71$ MeV, which is shown by the dotted line.

potential. The value of the modified potential at $x = x_c$ is $V_{\text{mod}}(x_c) = 4.21$ MeV, whereas, the barrier height is $V_b = V(x = 8.1 \text{ fm}) = 4.75$ MeV.

We solve the s.p. states of the modified Hamiltonian,

$$h_{\text{mod}}(x) = -\frac{\hbar^2}{2m} \frac{d^2}{dx^2} + V_{\text{mod}}(x), \quad (8)$$

as

$$h_{\text{mod}}(x)\phi_n(x) = \epsilon_n \phi_n(x). \quad (9)$$

In this paper, we assume that all the s.p. states with negative energy, that is, $\epsilon_n < 0$, are occupied by the core nucleus. Therefore, there is only one bound state in this potential at $\epsilon = 2.71$ MeV. The other positive energy states are in the continuum spectra, which we discretize with a box of $X_{\text{box}} = \pm 120$ fm. We have confirmed that the bound state at $\epsilon = 2.71$ MeV corresponds to a resonance state of the original potential, whose energy is stabilized against a variation of X_{box} [52–54].

By using these s.p. wave functions, one can obtain the eigenfunctions of the modified three-body Hamiltonian,

$$H_{\text{mod}}(x_1, x_2) = h_{\text{mod}}(x_1) + h_{\text{mod}}(x_2) + v_{\text{pp}}(x_1, x_2), \quad (10)$$

as

$$\Psi_k(x_1, x_2) = \sum_{n_1 \leq n_2} \alpha_{n_1 n_2}^{(k)} \Phi_{n_1 n_2}(x_1, x_2), \quad (11)$$

where we exclude those s.p. states occupied by the core nucleus. Here, $\Phi_{n_1 n_2}(x_1, x_2)$ is defined as

$$\Phi_{n_1 n_2}(x_1, x_2) = \frac{1}{\sqrt{2(1 + \delta_{n_1, n_2})}} [\phi_{n_1}(x_1)\phi_{n_2}(x_2) + \phi_{n_2}(x_1)\phi_{n_1}(x_2)] |S = 0\rangle. \quad (12)$$

Because we use spin-independent interactions in the Hamiltonian, the total spin S of the two protons is a good quantum number. We set it to be zero (that is, the spin-singlet state). The spatial part of the $2p$ wave function is, therefore, symmetric under the exchange of x_1 and x_2 . The coefficients $\alpha_{n_1 n_2}^{(k)}$ in Eq. (11) are determined by diagonalizing the Hamiltonian matrix for the modified Hamiltonian H_{mod} .

The next step is to carry out the time evolution for $t > 0$ by starting from the lowest eigenfunction of the modified Hamiltonian, i.e., $\Psi_{k=0}$ in Eq. (11) at the eigenenergy E_0 . That is,

$$\Psi(t = 0, x_1, x_2) = \Psi_0(x_1, x_2). \quad (13)$$

By excluding the core-occupied states in the expansion, we have confirmed that there is only one bound state for H_{mod} in the energy region between 0 and $2V_{\text{mod}}(x_c)$. Similar to a s.p. resonance state, the lowest state Ψ_0 corresponds to the three-body resonance state of the original Hamiltonian H . The energy E_0 corresponds to the resonance energy of the three-body system, that is, the Q value for the $2p$ decay.

We then solve the time-dependent Schrödinger equation with the original Hamiltonian H ,

$$i\hbar \frac{\partial}{\partial t} \Psi(t, x_1, x_2) = H\Psi(t, x_1, x_2) \quad (14)$$

$$= (H_{\text{mod}} + \Delta V)\Psi(t, x_1, x_2), \quad (15)$$

where

$$\Delta V = V(x_1) + V(x_2) - V_{\text{mod}}(x_1) - V_{\text{mod}}(x_2) \quad (16)$$

is the difference between the original and the modified potentials. We expand the time-dependent $2p$ wave function with the eigenfunctions of the modified Hamiltonian, that is, $\Psi_k(x_1, x_2)$ given in Eq. (11) as

$$\Psi(t, x_1, x_2) = \sum_k c_k(t) \Psi_k(x_1, x_2), \quad (17)$$

with the initial condition of

$$c_k(t = 0) = \delta_{k,0}. \quad (18)$$

By substituting Eq. (17) into Eq. (15) and by using the orthogonality of Ψ_k , we obtain the differential equation for the expansion coefficients $c_i(t)$,

$$i\hbar \frac{dc_i(t)}{dt} = \langle \Psi_i | H | \Psi \rangle \quad (19)$$

$$= \sum_k c_k(t) (E_i \delta_{i,k} + \langle \Psi_i | \Delta V | \Psi_k \rangle). \quad (20)$$

By using the wave function so obtained, one can compute the survival probability $P_s(t)$ and the decay width Γ as [34–38]

$$P_s(t) \equiv |\langle \Psi_0 | \Psi(t) \rangle|^2 = |c_0(t)|^2, \quad (21)$$

$$\Gamma = -\hbar \frac{\dot{P}_s(t)}{P_s(t)}. \quad (22)$$

When the survival probability is an exponential function of t , the decay width Γ becomes a constant. In the next section, we show that $P_s(t)$, indeed, has an exponential form after a sufficient time evolution.

III. RESULTS

A. Decay energy and width

Before we numerically solve the time-dependent Schrödinger equation, let us first investigate the overlaps between the initial wave function Ψ_0 and the eigenfunctions of the original Hamiltonian H . That is,

$$Q_k \equiv |\langle \tilde{\Psi}_k | \Psi_0 \rangle|^2, \quad (23)$$

where $|\tilde{\Psi}_k\rangle$ is the eigenfunctions of the original Hamiltonian, which satisfies

$$H|\tilde{\Psi}_k\rangle = \tilde{E}_k|\tilde{\Psi}_k\rangle. \quad (24)$$

Figure 2 shows the overlaps Q_k as a function of \tilde{E}_k for $g = 0$ and 20 MeV fm. The initial state is fragmented over several eigenfunctions of the original Hamiltonian and, thus, forms a wave packet, which evolves in time. As one can see, the fragmentation of the initial state is small where the energy spreading corresponds to the decay width.

Let us now numerically solve the time-dependent Schrödinger equation. To this end, we use a time mesh of $\Delta t = 0.01$ fm/c. Figure 3 shows the survival probability and the decay width defined as Eqs. (21) and (22) as a function of time t for several values of g . One can see that the decay width converges to a constant value after sufficient time evolution,

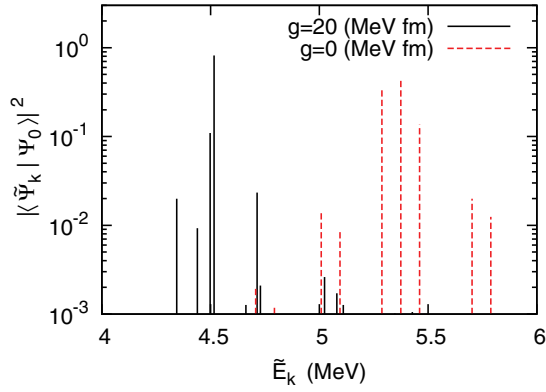


FIG. 2. (Color online) Overlaps between the initial state Ψ_0 and the eigenfunctions $\tilde{\Psi}_k$ of the original three-body Hamiltonian as a function of the corresponding eigenenergies \tilde{E}_k . The solid and the dashed lines correspond to the cases of $g = 20$ and 0 MeV fm, respectively. Notice that the initial state is the lowest eigenstate of the modified Hamiltonian H_{mod} with the eigenenergy of 4.56 MeV (5.42 MeV) for $g = 20$ MeV fm ($g = 0$ MeV fm).

which indicates the exponential decay law $P_s(t) = e^{-i\Gamma t/\hbar}$. Notice that the converged values for the decay width with this model Hamiltonian are on the same order as the experimental width for ${}^6\text{Be}$ and ${}^{16}\text{Ne}$ [19–21,55]. At shorter periods, the decay width shows a transient behavior [34–38]. That is, the survival probability behaves like a parabolic function of t , whereas, the decay width increases linearly [56,57].

The dependence of the decay width on the strength of the pairing interaction is shown in Fig. 4(b). In Fig. 4(a), we also

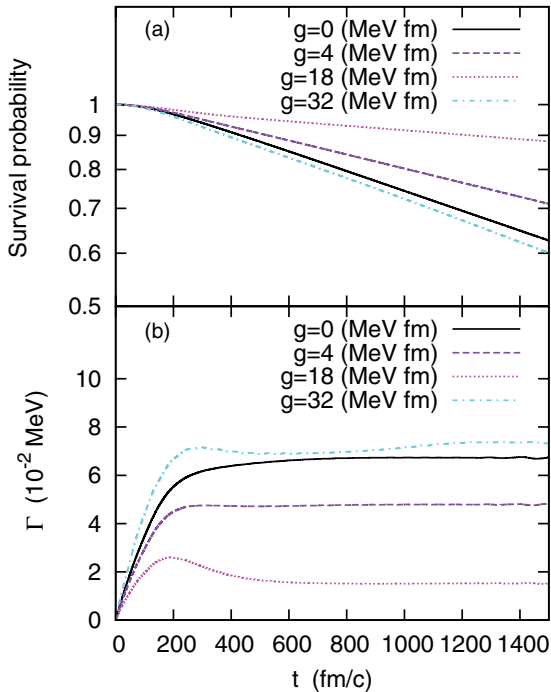


FIG. 3. (Color online) (a) The survival probability as a function of time t defined by Eq. (21). (b) The decay width defined by Eq. (22). These are plotted for several values of g indicated in the figure.

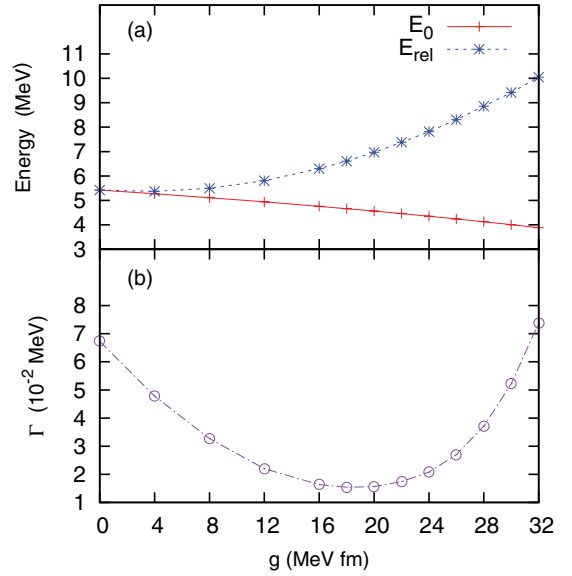


FIG. 4. (Color online) (a) The decay energy E_0 of the three-body system as a function of the strength of the pairing interaction g . The dashed line indicates the asymptotic kinetic energy of a bound diproton. (b) The decay width estimated at $t = 1200$ fm/c.

show the decay energy E_0 [that is, the eigenenergy of the modified Hamiltonian given by Eq. (10)] and the asymptotic kinetic energy of diproton E_{rel} defined as

$$E_{\text{rel}} = E_0 + B_{\text{pp}}, \quad (25)$$

where $B_{\text{pp}} = mg^2/4\hbar^2$ is the binding energy of a diproton. The decay width is estimated at $t = 1200$ fm/c where it has been well converged (see Fig. 3).

The decay width Γ first decreases as a function of g , despite that the diproton kinetic energy E_{rel} increases. This should be related to the decrease in the decay energy E_0 , which indicates that the sequential two-proton emissions are the main decay mechanism in this region of g , even though two protons are bound in this one-dimensional model. For $g \geq 18$ MeV fm, on the other hand, the decay width increases. This is consistent with the increase in E_{rel} , which suggests that the direct diproton decay, that is, the emission of a deeply bound diproton, is the main mechanism in this region.

The transition from the sequential to the diproton decays will be clarified more in the next subsection.

B. Two-particle density and flux distributions

To confirm a transition from a sequential to a simultaneous decay discussed in the previous subsection, we next discuss the time evolution of two-particle density distribution,

$$\rho(t, x_1, x_2) = |\Psi(t, x_1, x_2)|^2. \quad (26)$$

We also analyze the flux distribution defined as

$$j_i(t, x_1, x_2) = \frac{\hbar}{2im} \left(\Psi^* \frac{\partial \Psi}{\partial x_i} - \frac{\partial \Psi^*}{\partial x_i} \Psi \right) \quad (j = 1, 2). \quad (27)$$

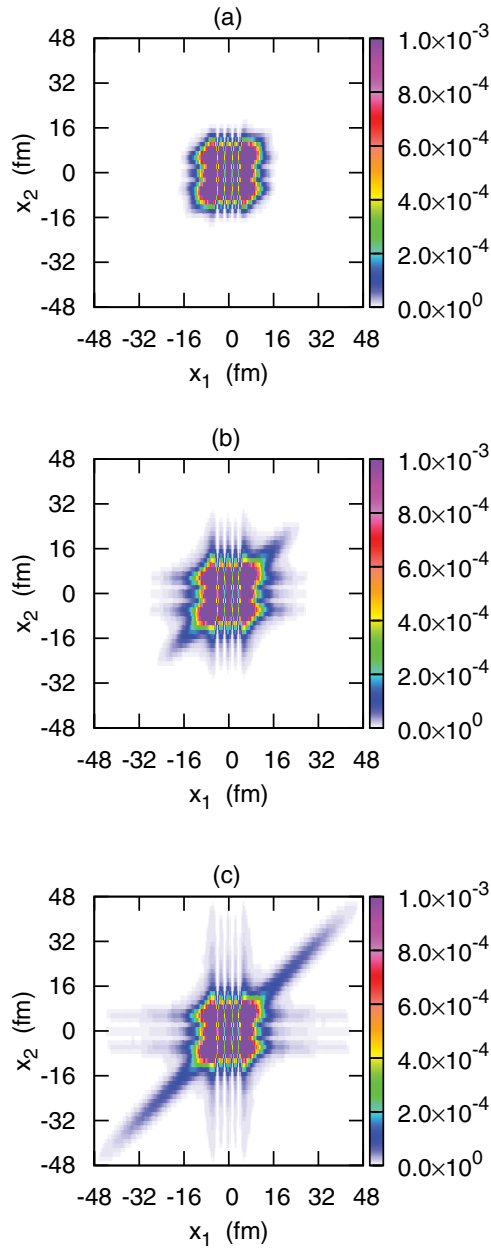


FIG. 5. (Color online) The time evolution of the density distribution $\rho(t, x_1, x_2)$ in the two-dimensional (x_1, x_2) plane calculated with the pairing strength of $g = 20$ MeV fm. Panels (a)–(c) correspond to the density at $t = 0, 300,$ and 600 fm/c, respectively.

Note that the $2p$ density is normalized as

$$\int_{-\infty}^{\infty} \rho(t, x_1, x_2) dx_1 dx_2 = 1. \quad (28)$$

Figures 5 and 6 show the two-particle density and flux distributions, respectively, for $g = 20$ MeV fm at $t = 0, 300,$ and 600 fm/c. The corresponding quantities for $g = 0$ are also shown in Figs. 7 and 8. The flux distributions are plotted in a form of vector at each value of (x_1, x_2) in the two-dimensional (x_1, x_2) plane where the core nucleus is located at the origin. Note that there is no flux distribution at $t = 0$ because the

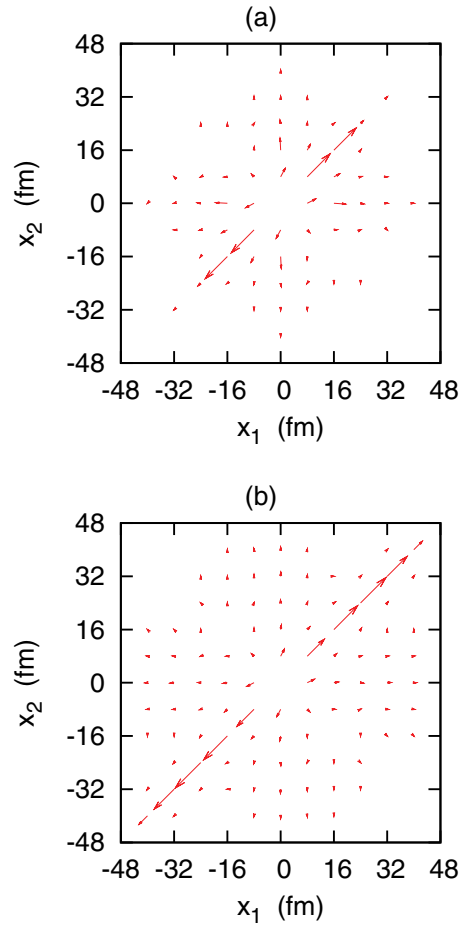
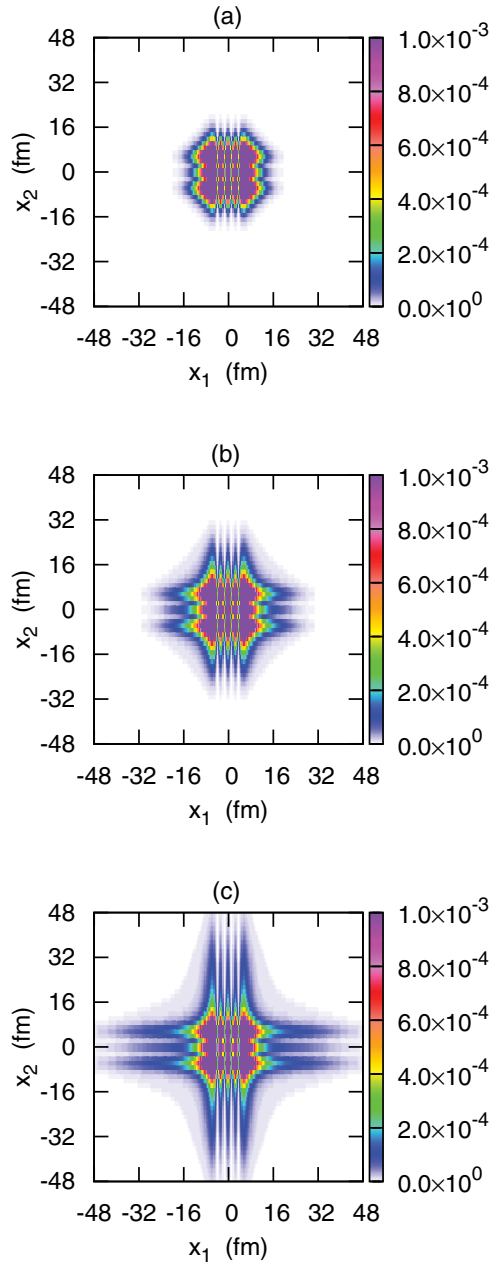


FIG. 6. (Color online) The flux distributions $\mathbf{j}(t, x_1, x_2) = j_1(t, x_1, x_2)\mathbf{e}_1 + j_2(t, x_1, x_2)\mathbf{e}_2$, where \mathbf{e}_i is the unit vector in the two-dimensional (x_1, x_2) plane. These are obtained with $g = 20$ MeV fm at (a) $t = 300$ fm/c and (b) 600 fm/c and are plotted in arbitrary units.

initial wave function $\Psi(t = 0)$ can be taken to be real, and we do not show it in the figures.

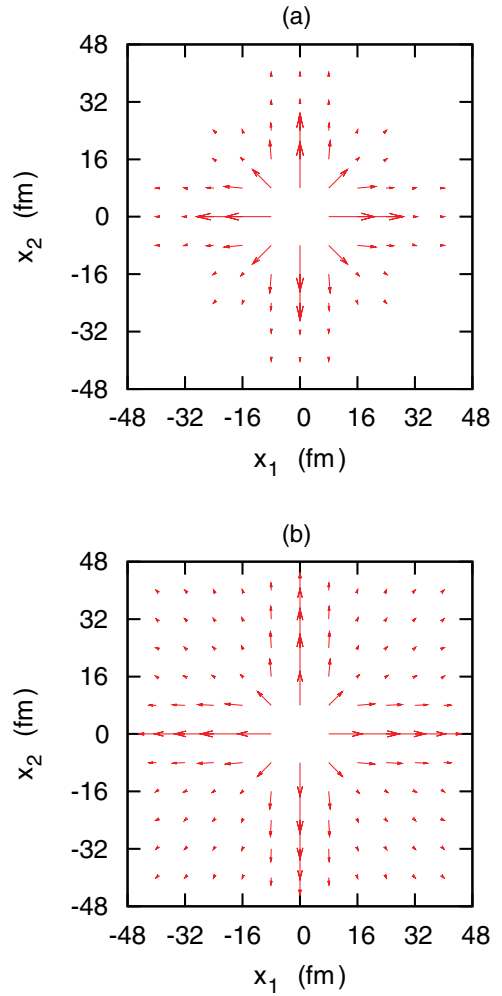
Figures 5(a) and 7(a) show the density distribution for the initial $2p$ state, which is confined within the modified potential V_{mod} . Because of the pairing correlation, the initial density for $g = 20$ MeV fm has an asymmetric form with the peaks along $x_1 = x_2$, which are higher than those along $x_1 = -x_2$ [42]. The peaks along the $x_1 = x_2$ line, that is, in the first and third quadrants of these panels, correspond to a compact diproton cluster. On the other hand, the peaks along the $x_1 = -x_2$ line (i.e., in the second and the fourth quadrants) correspond to a configuration in which two protons are located opposite the core nucleus. If we discard the pairing interaction, the density distribution has four symmetric peaks as shown in Fig. 7(a), that is, the probability in the first and third quadrants is the same as that in the second and fourth quadrants [42].

The effect of the pairing correlation is also apparent during the time evolution. In the presence of the pairing correlation, the extension of the two-particle density along the $x_1 = x_2$ line increases significantly, although the extension along the $x_1 = 0$ or $x_2 = 0$ lines is not negligible. This is in marked contrast with the uncorrelated case shown in Fig. 7 in which the two-particle density expands democratically. That is, in


 FIG. 7. (Color online) Same as Fig. 5 but for $g = 0$ MeV fm.

the uncorrelated case, the probability of emission of the two protons in opposite directions is equal to that in the same direction. The flux distributions shown in Figs. 6 and 8 also indicate the same behavior.

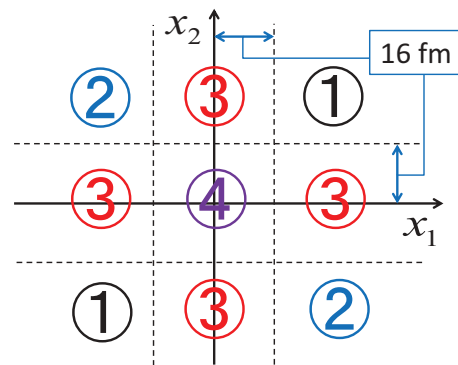
To investigate the time evolution more quantitatively, we divide the (x_1, x_2) plane into four regions shown in Fig. 9. That is, as follows: (i) the region of $x_1 > 16$ and $x_2 > 16$ fm as well as the region of $x_1 < -16$ and $x_2 < -16$ fm, (ii) the region of $x_1 > 16$ and $x_2 < -16$ fm as well as the region of $x_1 < -16$ and $x_2 > 16$ fm, (iii) the region of $-16 \leq x_1 \leq 16$ and $|x_2| > 16$ fm as well as the region of $-16 \leq x_2 \leq 16$ and $|x_1| > 16$ fm, and (iv) the rest in the (x_1, x_2) plane. At each time, we integrate the two-particle density distribution in each


 FIG. 8. (Color online) Same as Fig. 6 but for $g = 0$ MeV fm.

region,

$$P_k(t) = \int_{\text{region } k} \rho(t, x_1, x_2) dx_1 dx_2 \quad (k = 1-4). \quad (29)$$

The time evolution of these partial probabilities is shown in Fig. 10 for $g = 0, 20,$ and 32 MeV fm. We also show the total decay probability, that is, $1 - P_4 = P_1 + P_2 + P_3$.


 FIG. 9. (Color online) The four regions in the (x_1, x_2) plane used to calculate the partial probabilities shown in Fig. 10. The boundaries of each region are at $x_1 = \pm 16$ and $x_2 = \pm 16$ fm.

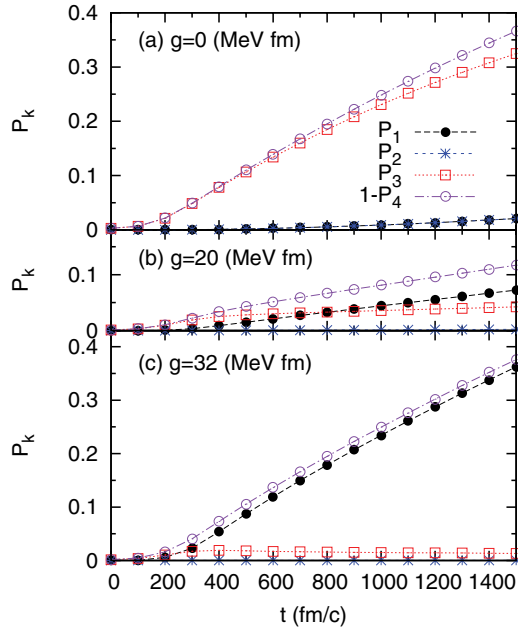


FIG. 10. (Color online) The time evolution of the partial probabilities in the regions defined in Fig. 9 for $g = 0, 20,$ and 32 MeV fm. The total decay probability $P_{\text{tot}} \equiv 1 - P_4 = P_1 + P_2 + P_3$ is also shown by the dot-dashed lines.

We first discuss the behavior for the uncorrelated case shown in Fig. 10(a). In this case, the dominant process is the decay into the third region P_3 , which corresponds to an emission of one of the valence protons, whereas, the other proton remains inside the core-proton potential. As there is no active s.p. bound state in the present core-proton potential, the second proton mainly occupies the s.p. resonance state. This resonance state eventually decays, and the second proton is emitted outside the potential after a sufficient time evolution. This is nothing but the sequential two-proton decay and can be clearly seen in the probabilities P_1 and P_2 , which exist only at $t \gtrsim 600$ fm/c. Notice that P_1 and P_2 are identical to each other since the second proton is emitted into either the left or the right direction with respect to the core nucleus with an equal probability irrespective of the position of the first proton.

For $g = 20$ MeV fm shown in Fig. 10(b), the probability in region (i) increases considerably due to the pairing correlation, whereas, P_3 decreases significantly. This partly corresponds to an emission of a bound diproton, that is, the simultaneous two-proton decay. Notice, however, that P_3 is still larger than P_1 at $t \lesssim 800$ fm/c, and a sequential decay also coexists for this value of g . As we have shown in Fig. 4, the total decay probability $P_1 + P_2 + P_3$ decreases compared to the uncorrelated case.

When the pairing interaction is even stronger, the simultaneous diproton decay becomes dominant. See Fig. 10(c) for $g = 32$ MeV fm. In this case, P_1 is the dominant part of the total decay probability, except for the short-time region . . .

which the high-energy components in the initial wave function quickly escape from the potential barrier. The long-time behavior in this case may correspond to α decays in realistic nuclei for which a tightly bound α particle tunnels through the Coulomb barrier of the daughter nucleus.

From these studies, it is evident that the present one-dimensional three-body model nicely describes a transition from an uncorrelated case to a strongly correlated case for many-particle tunneling decays.

IV. SUMMARY

We have employed the time-dependent method and have qualitatively investigated many-particle tunneling decays, particularly, the two-proton radioactivity. To this end, we used a one-dimensional three-body model, which consisted of a core nucleus and two valence protons. To describe the decaying process, we first confined the two-proton wave function inside a confining potential. The confining potential was then changed to the original potential with which the two-proton wave function evolved in time. We confirmed that the survival probability followed the exponential decay law after a sufficient time evolution, which yielded a constant decay width. We found that an emission of a bound diproton was enhanced due to the pairing correlation as was evidenced in the time evolution of the density and flux distributions. We have also analyzed the partial probabilities and have discussed the relative importance of the sequential and simultaneous two-proton decays. We showed that, for the uncorrelated case, the sequential decay was the dominant decay process, whereas, the simultaneous decay played an essential role in the case of strong pairing correlation. For an intermediate value of the pairing strength, we have shown that both the simultaneous and the sequential two-proton emissions coexist.

The one-dimensional three-body model, which we employed in this paper, is a simple schematic with which a deep understanding of many-particle decay process may be obtained. One drawback, however, is that two protons are inevitably bound, even with an infinitesimal attraction between the two protons. Even though our model nicely demonstrates the co-existence of the simultaneous and sequential decays for an intermediate pairing interaction, in reality, two protons are never bound in vacuum. It will be an important task to extend the present paper to realistic two-proton emitters in three dimensions, such as ${}^6\text{Be}$ and ${}^{16}\text{Ne}$ nuclei. Work towards this direction is in progress, and we will report on it in a separate paper.

ACKNOWLEDGMENTS

We thank D. Lacroix for useful discussions. This work was supported by the Global COE Program ‘‘Weaving Science Web beyond Particle-Matter Hierarchy’’ at Tohoku University and by the Japanese Ministry of Education, Culture, Sports, Science and Technology by a Grant-in-Aid for Scientific Research under the Program No. (C) 22540262.

[1] J. Bardeen, *Phys. Rev. Lett.* **6**, 57 (1961).

[2] C. A. Caldeira and A. J. Leggett, *Ann. Phys. (NY)* **149**, 374 (1983).

[3] V. V. Flambaum and V. G. Zelevinsky, *J. Phys. G* **31**, 335 (2005).

[4] C. A. Bertulani, V. V. Flambaum, and V. G. Zelevinsky, *J. Phys. G* **34**, 2289 (2007).

- [5] N. Ahsan and A. Volya, *Phys. Rev. C* **82**, 064607 (2010).
- [6] A. C. Shotter and M. D. Shotter, *Phys. Rev. C* **83**, 054621 (2011).
- [7] A. B. Balantekin and N. Takigawa, *Rev. Mod. Phys.* **70**, 77 (1998).
- [8] M. Dasgupta, D. J. Hinde, N. Rowley, and A. M. Stefanini, *Annu. Rev. Part. Sci.* **48**, 401 (1998).
- [9] R. Vandenbosch and J. R. Huizenga, *Nuclear Fission* (Academic, New York, 1974).
- [10] D. S. Delion, *Theory of Particle and Cluster Emission* (Springer-Verlag, Berlin, 2010).
- [11] C. A. Bertulani and P. Danielewicz, *Introduction to Nuclear Reactions* (Institute of Physics, London, 2004).
- [12] I. J. Thompson and F. M. Nunes, *Nuclear Reactions for Astrophysics* (Cambridge University Press, Cambridge, UK, 2009).
- [13] K. Sasaki, K. Suekane, and I. Tonzuka, *Nucl. Phys. A* **147**, 45 (1970).
- [14] I. Tonzuka and A. Arima, *Nucl. Phys. A* **323**, 45 (1979).
- [15] K. Varga and R. J. Liotta, *Phys. Rev. C* **50**, R1292 (1994).
- [16] M. Pfützner *et al.*, *Eur. Phys. J. A* **14**, 279 (2002).
- [17] J. Giovinazzo *et al.*, *Phys. Rev. Lett.* **89**, 102501 (2002).
- [18] K. Miernik *et al.*, *Phys. Rev. Lett.* **99**, 192501 (2007).
- [19] O. V. Bochkarev *et al.*, *Nucl. Phys. A* **505**, 215 (1989).
- [20] L. V. Grigorenko, R. C. Johnson, I. G. Mukha, I. J. Thompson, and M. V. Zhukov, *Phys. Rev. C* **64**, 054002 (2001).
- [21] L. V. Grigorenko *et al.*, *Phys. Rev. C* **80**, 034602 (2009).
- [22] M. Pfützner, M. Karny, L. V. Grigorenko, and K. Riisager, *Rev. Mod. Phys.* **84**, 567 (2012).
- [23] B. Blank and M. Ploszajczak, *Rep. Prog. Phys.* **71**, 046301 (2008).
- [24] L. V. Grigorenko, *Phys. Part. Nuclei* **40**, 674 (2009), and references therein.
- [25] L. V. Grigorenko, T. D. Wiser, K. Mercurio, R. J. Charity, R. Shane, L. G. Sobotka, J. M. Elson, A. H. Wuosmaa, A. Banu, M. McCleskey, L. Trache, R. E. Tribble, and M. V. Zhukov, *Phys. Rev. C* **80**, 034602 (2009).
- [26] M. Matsuo, K. Mizuyama, and Y. Serizawa, *Phys. Rev. C* **71**, 064326 (2005).
- [27] M. Matsuo, *Phys. Rev. C* **73**, 044309 (2006).
- [28] K. Hagino and H. Sagawa, *Phys. Rev. C* **72**, 044321 (2005).
- [29] T. Oishi, K. Hagino, and H. Sagawa, *Phys. Rev. C* **82**, 024315 (2010).
- [30] A. Spyrou *et al.*, *Phys. Rev. Lett.* **108**, 102501 (2012).
- [31] M. Grasso, D. Lacroix, and A. Vitturi, *Phys. Rev. C* **85**, 034317 (2012).
- [32] G. Scamps, D. Lacroix, G. F. Bertsch, and K. Washiyama, *Phys. Rev. C* **85**, 034328 (2012).
- [33] G. Potel, F. Barranco, E. Vigezzi, and R. A. Broglia, *Phys. Rev. Lett.* **105**, 172502 (2010); G. Potel, F. Barranco, F. Marini, A. Idini, E. Vigezzi, and R. A. Broglia, *ibid.* **107**, 092501 (2011).
- [34] O. Serot, N. Carjan, and D. Strottman, *Nucl. Phys. A* **569**, 562 (1994).
- [35] P. Talou, N. Carjan, and D. Strottman, *Phys. Rev. C* **58**, 3280 (1998).
- [36] P. Talou, N. Carjan, and D. Strottman, *Nucl. Phys. A* **647**, 21 (1999).
- [37] P. Talou, D. Strottman, and N. Carjan, *Phys. Rev. C* **60**, 054318 (1999).
- [38] P. Talou, N. Carjan, C. Negrevergne, and D. Strottman, *Phys. Rev. C* **62**, 014609 (2000).
- [39] A. del Campo, *Phys. Rev. A* **84**, 012113 (2011).
- [40] G. García-Calderón and L. G. Mendoza-Luna, *Phys. Rev. A* **84**, 032106 (2011).
- [41] C. N. Davids and H. Esbensen, *Phys. Rev. C* **61**, 054302 (2000).
- [42] K. Hagino *et al.*, *J. Phys. G* **38**, 015105 (2011).
- [43] M. S. Pindzola, D. C. Griffin, and C. Bottcher, *Phys. Rev. Lett.* **66**, 2305 (1991).
- [44] R. Grobe and J. H. Eberly, *Phys. Rev. Lett.* **68**, 2905 (1992); *Phys. Rev. A* **48**, 4664 (1993).
- [45] M. Lein, E. K. U. Gross, and V. Engel, *Phys. Rev. Lett.* **85**, 4707 (2000).
- [46] T. Oishi, K. Hagino, and H. Sagawa, *Phys. Rev. C* **84**, 057301 (2011).
- [47] H. Nakada and M. Yamagami, *Phys. Rev. C* **83**, 031302(R) (2011).
- [48] E. Merzbacher, *Quantum Mechanics*, 3rd ed. (Wiley, New York, 1998); S. Gasiorowicz, *Quantum Physics*, 3rd ed. (Wiley, New York, 2003).
- [49] S. A. Gurvitz and G. Kalbermann, *Phys. Rev. Lett.* **59**, 262 (1987).
- [50] S. A. Gurvitz, *Phys. Rev. A* **38**, 1747 (1988).
- [51] S. A. Gurvitz, P. B. Semmes, W. Nazarewicz, and T. Vertse, *Phys. Rev. A* **69**, 042705 (2004).
- [52] A. U. Hazi and H. S. Taylor, *Phys. Rev. A* **1**, 1109 (1970).
- [53] C. H. Maier, L. S. Cederbaum, and W. Domcke, *J. Phys. B* **13**, L119 (1980).
- [54] L. Zhang *et al.*, *Phys. Rev. C* **77**, 014312 (2008).
- [55] I. Mukha *et al.*, *Phys. Rev. C* **77**, 061303(R) (2008).
- [56] K. Grotz and H. V. Klapdor, *Phys. Rev. C* **30**, 2098 (1984).
- [57] M. Pons, D. Sokolovski, and A. del Campo, *Phys. Rev. A* **85**, 022107 (2012).